Bulgarian Chemical Communications, Volume 57, Issue 4 (pp. 309-318) 2025 DOI: 10.34049/bcc.57.4.5677

Computational study of propane dehydrogenation into propylene over chromium oxide *via* a combined use of central composite design & microkinetic simulation

T. Oyegoke*

CEPRIs – CAD Engineering of Processes & Reactive Interfaces Group, Chemical Engineering Department, Ahmadu Bello University, Zaria 234, Nigeria

Received: November 3, 2024, Revised: September 13, 2025

The global demand for propylene continues to increase due to its extensive application in the production of petrochemicals. While fluid catalytic cracking (FCC) remains a major source of propylene, the growing need for targeted production has directed attention to on-purpose processes such as propane dehydrogenation (PDH). However, PDH performance is often hindered by low propylene yields, especially when chromium oxide is used as the catalyst. In this study, microkinetic modeling was integrated with central composite design (CCD) to evaluate the influence of flow rate, pressure, catalyst porosity, and temperature on the kinetics of propane dehydrogenation over chromium oxide. Rate-control analysis was further employed to identify the kinetically relevant steps governing the overall reaction rate. The results demonstrate that increases in flow rate (-5.69%), pressure (-9.28%), and porosity (-62.40%) reduce the reaction rate, whereas temperature (+22.63%) elevation enhances it, confirming the endothermic nature of the reaction. Among all variables, catalyst porosity exhibited the highest influence (-62.40%) on the reaction rate, while flow rate had the least (+5.69%). Rate-control analysis revealed that the first hydrogen abstraction step is the rate-determining transition state ($X_{TRC,TS} = -4$), and adsorbed propane is the rate-controlling intermediate ($X_{TRC,IS} = +4$). These findings suggest that improving catalyst porosity and introducing suitable promoters could lower the energy barrier of the rate-limiting step or destabilize the intermediate, thus enhancing the overall reaction rate beyond what is attainable through thermodynamic optimization alone.

Keywords: Dehydrogenation, Olefins, Paraffins, Microkinetics, Density Functional Theory, Modeling.

INTRODUCTION

Dehydrogenation is a crucial value-adding process that converts paraffins into olefins, which are key building blocks for the chemical industries due to their high reactivity [1]. Propylene, in particular, is one of the most valuable olefins, serving as an essential feedstock for the production of a wide range of petrochemical products, including polypropylene, isopropanol, propylene oxide, acrylonitrile, and many other useful materials [2, 3].

Traditionally, steam cracking and fluid catalytic cracking (FCC) processes [4–6] have been the primary sources through which the bulk of the propylene consumed in the industries was produced. However, only a small fraction of the global propylene supply currently comes from the on-purpose method, otherwise known as propane dehydrogenation [7, 8]. Recent development, particularly the decline or drop in the price of shale gas, have renewed the interest in the propane dehtydrogenation technologies. This shift is further supported by the rising post-pandemic demand for propylene in the petrochemical sector. As a result, there is a growing need to enhance propylene yield and selectivity in the dehydrogenation propane into propylene, which is often hindered by challenges such as low conversion rates and poor selectivity of conventional catalysts like platinium (Pt) and chromium oxide used in the conversion processes [7].

Several studies [4, 8–32] have explored various strategies to overcome these limitations. For example, Rimax *et al.* [33] improved the stability and selectivity of platinium-based catalysts for propylene production by alloying Pt with germanium (Ge). In another study, Yang *et al.* [34] demonstrated that incorporating magnesium oxide into a gallium-based catalyst supported on ZSM-5 increased propylene selectivity to 90.80%. A review of the literature indicates that most studies have focused on metallic catalysts [30, 35–38] — particularly platinum — for propane dehydrogenation. In contrast, metal oxides such as chromium oxide have received relatively less attention in computational investigations. Among the few existing studies, Kim *et al.* [39] reported that enhancing the lattice oxygen content of chromium oxide (CrO) catalysts significantly improved their

* To whom all correspondence should be sent:
E-mail: *OyegokeToyese@gmail.com*

catalytic performance in the propane dehydrogenation process.

These findings of Kim *et al*. aligned with the previous computational studies [15, 26] on propane dehydrogenation on CrO surface, which showed that the chromium (Cr) sites on the CrO catalysts are highly reactive and more abundant on the catalyst surface than the oxygen (O) sites. The Cr-sites dominance may hinder propylene desorption, potentially resulting in deep dehydrogenation and possible cracking of propylene to produce undesired products like ethylene, methane, and other lighter hydrocarbons due to the domination of the Cr-site, according to the established literature [25].

To support fuIO methods, this work addresses the challenge of low yields commonly reported for chromium oxide (CrO) catalysts [7], as well as the limited number of computational studies focused on this material. A combined approach involving microkinetic modeling and central composite design (CCD) was employed to examine the effects of flow rate, pressure, porosity, and temperature on the kinetics of propane dehydrogenation over chromium oxide. Unlike the traditional one-factor-at-a-time (OFAT) method, CCD enables effective quantification of the individual and interactive contributions of these parameters to the rate of propane conversion to propylene in the presence of the catalyst. Additionally, rate-control analysis was performed to evaluate the influence of individual reaction steps on the overall reaction kinetics. The investigation employed density functional theory (DFT) energies previously computed for the propane dehydrogenation process over chromium oxide in earlier work [26], where the underlying reaction mechanism was elucidated (as shown in Figure 1) for the conversion of propane to propylene on the catalyst surface. The findings identify key reaction steps—particularly those highlighted by the rate-control analysis—that can be further explored to improve catalyst performance during the design and synthesis of next-generation chromium-based catalysts.

COMPUTATIONAL METHOD

Kinetic modeling & simulation of propane dehydrogenation

The kinetics of propane dehydrogenation to propylene over chromium oxide was modeled using a microkinetic simulation approach, supported by relevant computational tools. This study aimed to identify the key parameters governing the reaction rate. A schematic overview of the simulation approach is presented in Figure 2. The details of the density functional theory (DFT) calculations used to obtain the energy profiles for the elementary steps have been reported in our previous work [26].

Elementary adsorption, desorption, and surface reaction rate

The elementary reaction rates for the various steps in the propane dehydrogenation mechanism—from initiation to termination—were incorporated into the reaction network. However, less stable intermediate states involved in certain steps were excluded from the modeling. The elementary reaction rates used in the simulation are summarized in Table 1.

The rate constants were calculated using the mathematical model presented in Equation (1):

$$k_i = P_{corr} * (k_B * T/h) * exp\left(-G^{\#}/RT\right) \quad (1)$$

where R_{fi} or R_{bi} is the reaction rate, P is the pressure, X is the surface site concentration (i.e., normalized form), k is the rate constant, P_{corr} is the correction term expressed in the model presented in Equation (2):

$$P_{corr} = {P_0}^{-N_{ns}} * X_0^{1-N_s} \quad (2)$$

$G^{\#}$ is the reaction activation energy computed using the expression presented in Equation (3):

$$G^{\#} = G_{TS} - G_R \quad (3)$$

Po is the standard pressure, T is the reaction temperature, X_o is the standard surface concentration obtained from the literature reports [40–42], R is the gas constant, k_B is the Boltzmann constant, h is the Planck constant, N_s is the surface species stoichiometric coefficient, N_{ns} is the non-surface species stoichiometric coefficient, X is the empty surface site concentration, and X_i is the species (i) surface site concentration.

Surface reaction activity models

Here, the surface reaction activities displaying the evolution, transformation, and disappearance of surface species during propane dehydrogenation into propylene over a chromium oxide catalyst were expressed in the following equations [43].

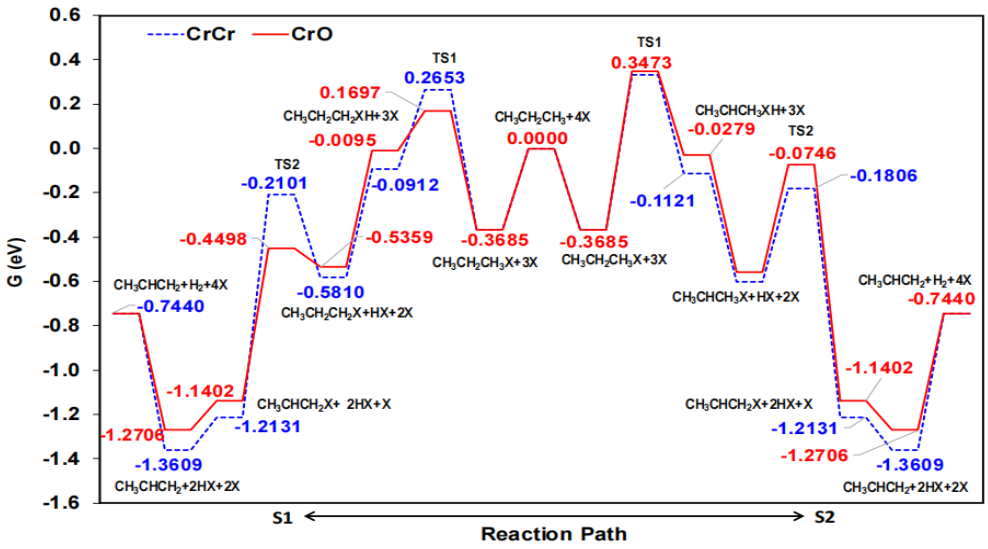

Figure 1. Propane dehydrogenation reaction mechanism across Cr-Cr and Cr-O pair sites with the energy profile using the reaction schemes 1 (LHS) and 2 (RHS) (all in eV), where LHS is the left-hand side, RHS is the right-hand side [26].

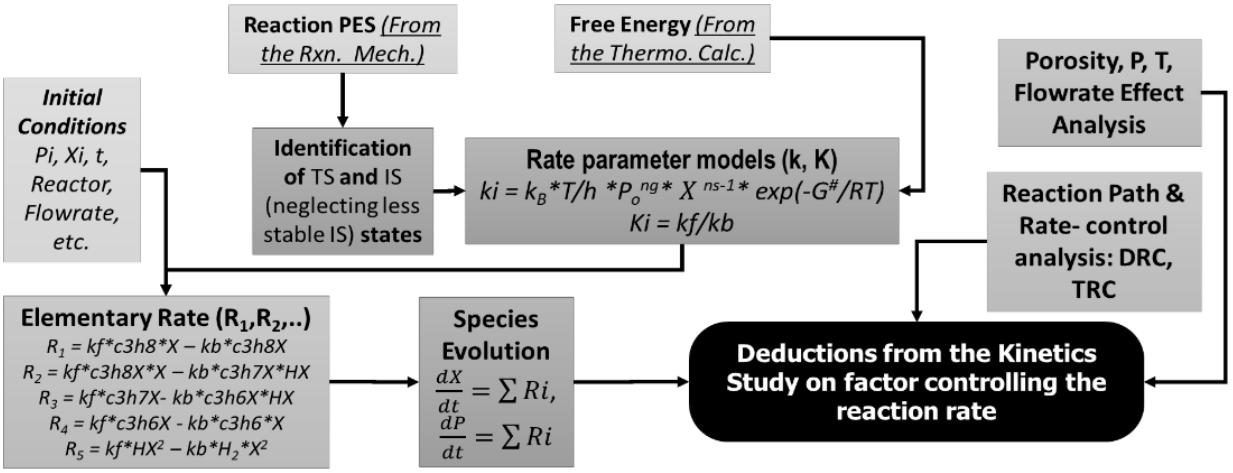

Figure 2. Flow chart showing the approach employed in the kinetics simulation

Table 1. List of elementary steps, including the rate expression for the backward & forward.

Elementary step	Forward reaction rate	Backward reaction rate
Propane adsorption	$R_{f1} = k_{f1} * P_{C3H8} * X$	$R_{b1} = k_{b1} * X_{C3H8}$
First hydrogen abstraction	$R_{f2} = k_{f2} * X_{C3H8} * X$	$R_{b2} = k_{b2} * X_{C3H7} * X_H$
Second hydrogen abstraction	$R_{f3} = k_{f3} * X_{C3H7} * X$	$R_{b3} = k_{b3} * X_{C3H6} * X_H$
Propylene adsorption	$R_{f4} = k_{f4} * X_{C3H6}$	$R_{b4} = k_{b4} * P_{C3H6} * X$
Hydrogen adsorption	$R_{f5} = k_{f5} * {X_H}^2$	$R_{b5} = k_{b5} * P_{H2} * X^2$

The expression for the evolution, transformation and disappearance of the adsorbed propane is presented in Equation (4):

$$\frac{dS_{C3H8}}{dt} = \frac{1}{X_{t=0}} \frac{dX_{C3H8}}{dt} = \frac{1}{X_{t=0}} \sum R_i \quad (4)$$

The expression for the propyl evolution, transformation, and disappearance in the reaction network is presented in Equation (5):

$$\frac{dS_{C3H7}}{dt} = \frac{1}{X_{t=0}} \sum R_i \quad (5)$$

The expression for the evolution, transformation and disappearance of propylene in the reaction network is presented in Equation (6):

$$\frac{dS_{C3H6}}{dt} = \frac{1}{X_{t=0}}\frac{dX_{C3H6}}{dt} = \sum R_i \quad (6)$$

The expression for the evolution, transformation and disappearance of hydrogen in the reaction network is presented in Equation (7):

$$\frac{dS_{H2}}{dt} = \frac{1}{X_{t=0}}\sum R_i \quad (3)$$

where $X_{t=0}$ is the initial surface concentration at time t=0, S_{H2} is the normalized surface concentration expressed as a function of $\frac{X_{C3H8}}{X_{t=0}}$ and $\sum R_i$is the overall reaction rate for the concerned species.

Reactor models

A choice of continuous stirred-tank reactor model (CSTR) [44, 45] was made for the microkinetic simulation in this study. A set of ordinary differential equations (ODEs) are used in modeling the rate of propane conversion (i.e., R), propylene production (i.e., P), and hydrogen production (i.e., H_2) are presented here to understand kinetics involved in the process. The reactor was set to an exit and inlet flowrate, Uo of 0.15 m^3/s for the processing of 1 m^3 of propane (Vp) into propylene, while the reactor volume, Vr, was obtained as a function of $n_{feed}Nk_B\frac{T_{reactor}}{P_{reactor}}$ and the amount of feed is expressed in the form $Vp\frac{Po}{RT}$ for propane charged into the reactor.

- *Propane disappearance model.* The prediction model for the propane disappearance rate with time as the reaction progresses is expressed in Equations (8a) and (8b):

$$\frac{dP_{C3H8}}{dt} = (1-\Phi)\frac{n_{feed}RT}{Xo\,Vr}\left(-R_{f1}+R_{b1}\right) + \frac{Uo}{Vr}\left(P_{C3H8,0}-P_{C3H8}\right) \quad (8a)$$

$$\frac{dY_{C3H8}}{dt} = \frac{1}{P_{t=o}}\frac{dP_{C3H8}}{dt} = (1-\Phi)\frac{n_{feed}RT}{P_{t=o}\,Xo\,Vr}\left(-R_{f1}+R_{b1}\right) + \frac{Uo}{Vr\,P_{t=o}}\left(P_{C3H8,0}-P_{C3H8}\right) \quad (4b)$$

- *Propylene appearance model.* The propylene appearance or production rate is expressed in Equation (9):

$$\frac{dY_{C3H6}}{dt} = (1-\Phi)\frac{n_{feed}RT}{P_{t=o}Xo\,Vr}\left(-R_{f5}+R_{b5}\right) + \frac{Uo}{Vr\,P_{t=o}}\left(P_{C3H6,0}-P_{C3H6}\right) \quad (9)$$

- *Hydrogen appearance model.* The hydrogen production rate is expressed in Equation (10):

$$\frac{dY_{H2}}{dt} = (1-\Phi)\frac{n_{feed}RT}{P_{t=o}Xo\,Vr}\left(-R_{f4}+R_{b4}\right) + \frac{Uo}{Vr\,P_{t=o}}\left(P_{H2,0}-P_{H2}\right) \quad (5)$$

where Vr is the reactor volume, Uo is the flow rate, $P_{X,0}$ is the inlet pressure, P_X is the exit pressure for specie X, Φ is the catalyst porosity. $P_{t=o}$ is the initial propane pressure at time t=0, Y_{H2} is the normalized surface concentration expressed as a function of $\frac{P_{H2}}{P_{t=0}}$ and $\sum R_i$is the overall reaction rate for the concerned species.

Rate-control analysis

The thermodynamic rate control, X_{TRC} models (at a steady equilibrium constant) [46, 47] in Equations (11) and (12) were employed to analyze the reaction paths to understand the influence of the respective reaction steps and states involved in the reaction.

$$X_{TRC,TS} = \frac{dln(R_{C3H8})}{d(G_{TS,i}/RT)} \quad (6)$$

$$X_{TRC,IS} = \frac{dln(R_{C3H8})}{d(G_{IS,i}/RT)} \quad (7)$$

where R_{C3H8} is the propylene rate of production, R is the gas constant, Gi denotes the respective energy states, while the production rate is expressed as $\frac{Uo}{Vr}\left(\frac{\Delta P_i}{P_{t=0}}\right)$ in 1/s. The model for X_{TRC} employed in this study was adopted from the literature. This analysis would identify the transition state (TS) and intermediate state (IS) greatly influencing the reaction rate, which would have to be explored to improve the catalyst performance.

Effect of temperature, pressure, flow rate and catalyst porosity on the reaction kinetics

The impact of temperature, pressure, flow rate, and catalyst porosity on the dehydrogenation process in the presence of the catalyst was evaluated using the central composite design (CCD) technique within the response surface methodology (RSM) framework. This was done to assess both the individual and interactive effects of the aforementioned factors on the reaction kinetics. The contributions of each factor were reported in percentage terms. Temperature, pressure, flow rate, and catalyst porosity were selected as study variables within a narrow range, where higher yield and selectivity had been previously observed in process simulation studies [31, 32]. These prior simulations evaluated the influence of temperature and pressure on product distribution in the absence of catalyst

effects. The current study used the propylene yield, obtained by solving the models presented earlier in Equations (8–10) using Python, as the response variable.

Statistical evaluation of the selected parameters' effects and contributions to the kinetics of the reaction process

The effects and contributions of the selected parameters like temperature, pressure, porosity, and reactor flowrate were evaluated using the central composite design (CCD) of the response surface methodology (RSM). The investigation was carried out within the following factor levels of 581 to 650 *°C* for temperature, 0.2 to 1.0 atm for pressure, and 0.15 to 0.20 *m³/s* for flow rate, with reference to the previous related studies [31, 32]. As for the porosity, the range of 0.50 to 0.99 was evaluated due to the fact that porosity lower than 0.5 can potentially contribute to mass transfer problem and high pressure drop, according to the literature report [45]. The results obtained from the analysis were compiled and reported.

RESULTS AND DISCUSSION

Kinetic modeling & simulation of propane dehydrogenation

The kinetics of the dehydrogenation process was modeled and simulated in a continuously stirred tank reactor (CSTR) operated for 1200 sec (i.e., 20 min) in the presence of chromium oxide catalyst. The baseline operating conditions were set at 581 °C, 1 atm pressure, with a catalyst porosity of 0.99 and a reactor inlet/outlet flow rate of 0.15 m³/s. The effects of varying key parameters were investigated: temperature (400–650 °C), pressure (0.2–1.0 atm), flow rate (0.15–0.20 m³/s), and porosity (0.50–0.99). The process was modeled to simulate the conversion of 1 m³ of propane in the reactor, with the reactor volume estimated using the ideal gas law model (nRT/P). The results obtained, including those from the rate-control analysis, are presented in the subsequent sections.

Effect of pressure on the reaction kinetics

The results collected to evaluate the effects of pressure on the reaction kinetics are presented in Figure 3, showing the results collated for pressures of 0.2 and 1.0 atm.

The results indicate that increasing the pressure from 0.2 to 1.0 atm negatively affects the reaction kinetics, as evidenced by the decrease in propane conversion and propylene yield from 71% to 43%, as shown in Figure 3 (production profile). Further analysis of the surface profiles in Figure 3 reveals that the adsorbed propane species (C_3H_8X) remained largely stable for an extended period before the transition point at which the adsorbed hydrogen species (HX) became more stable than the adsorbed propane. However, the stability of adsorbed hydrogen (HX) was observed to be more pronounced at lower pressures and significantly reduced at higher pressures.

Effect of temperature on the reaction kinetics

The results obtained for the temperature's impact on the reaction's kinetics evaluated in the presence of a chromium oxide catalyst are presented in Figure 4, where the production and surface profiles were reported for 400, 581, and 650 °C for a fixed period of reaction time.

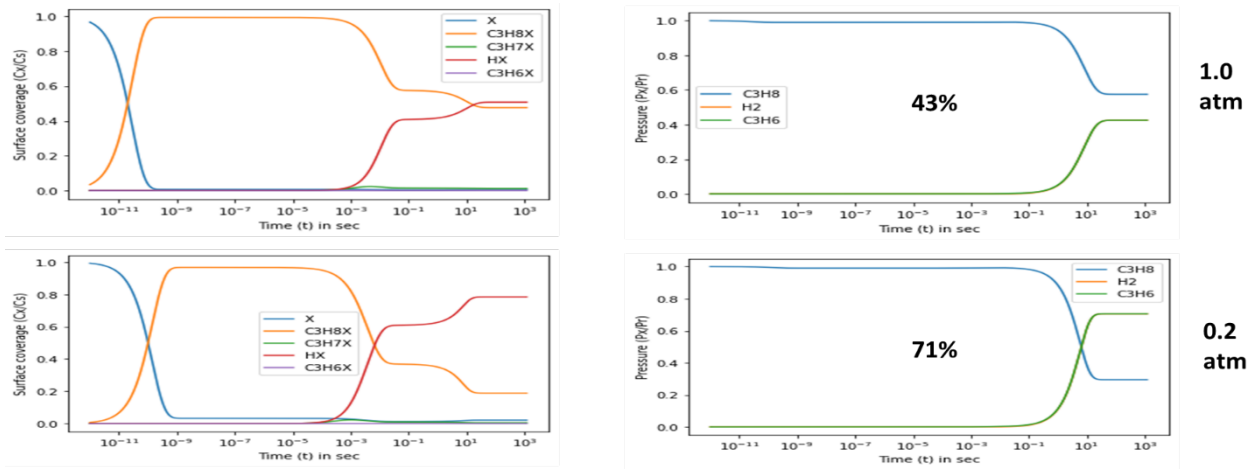

(a) (b)

Figure 3. Impact of reaction pressure (from 0.2 to 1 atm) on the reaction kinetics: (a) surface profile for surface species, and (b) production profile for non-surface species.

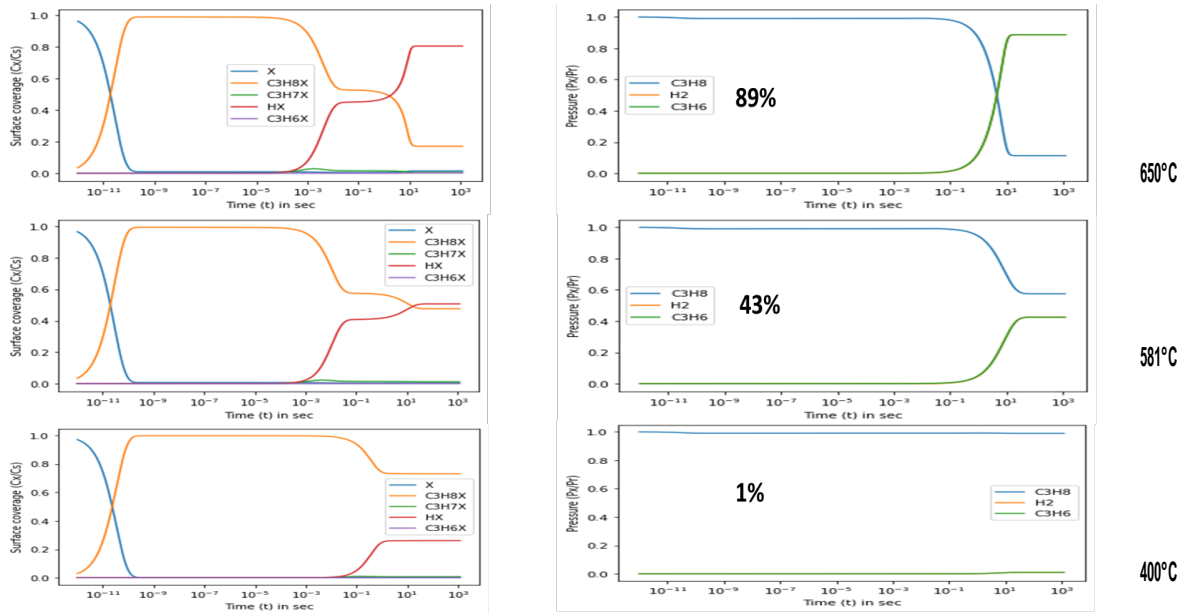

(a) (b)

Figure 4. Impact of reaction temperature (from 400 to 650 °C) on the reaction kinetics: (a) surface profile for surface species, and (b) production profile for non-surface species.

The analysis of the results presented in Figure 4, evaluating the effect of temperature on the reaction kinetics, shows that increasing the temperature from 400 °C to 650 °C significantly enhances the propylene yield, rising from 1% to 89%. The yield observed at 400 °C was the lowest among all the temperature levels considered in this study. This suggests that low temperatures are unfavorable for promoting the dehydrogenation reaction, which agrees with values reported in the literature [7,13,48–50], confirming that 550 °C is the minimum temperature favorable for the dehydrogenation of propane to propylene.

Effect of reactor flow rate on the reaction kinetics

The results evaluating the impact of reactor flow rate on the kinetics of propane dehydrogenation to propylene are presented in Figure 5, where both the production and surface profiles were assessed at flow rates of 0.15 and 0.20 m^3/s. The analysis indicates that increasing the flow rate in the CSTR from 0.15 to 0.20 m^3/s leads to a decrease in propylene yield from 43% to 30%. These findings reveal that a lower flow rate extends the residence time within the reactor, resulting in a higher yield, which is consistent with trends reported in the literature [51, 52].

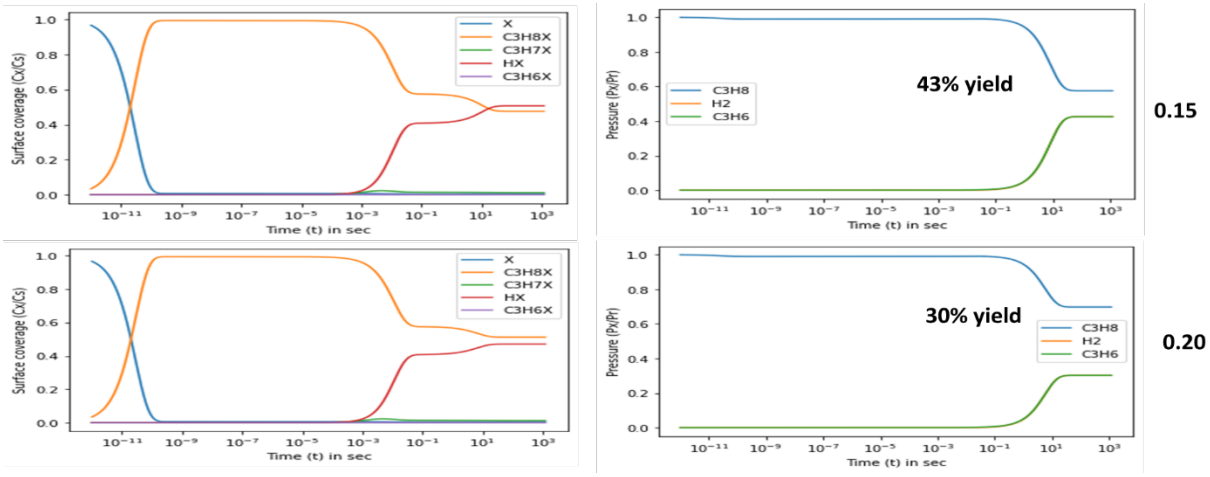

(a) (b)

Figure 5. Impact of reactor flow rate (from 0.15 to 0.20 squared meter per second) on the reaction kinetics: (a) the surface profile for surface species, and (b) the production profile for non-surface species.

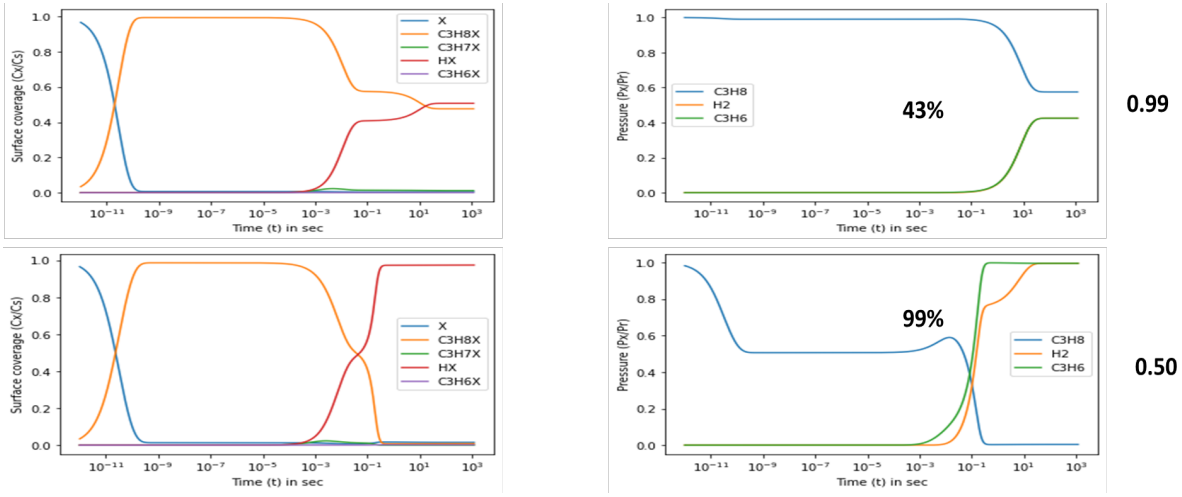

Figure 6. Impact of catalyst porosity (from 0.50 to 0.99) on the reaction kinetics: (a) the surface profile for surface species, and (b) the production profile for non-surface species.

Analysis of the surface profiles reported in Figure 5 unveils that the adsorbed propane (i.e., C_3H_8X) was largely stable. In contrast, the adsorbed hydrogen (i.e., HX) was partially stable for an extended period on the surface profiles before the transition time. Further study of the surface profile confirms that the reactor flow rates' change did not significantly affect the surface profile trend.

Effect of catalyst porosity on the reaction kinetics

The role of the catalyst porosity on the reaction kinetics was investigated. The results collected are presented in Figure 6, where its impacts on the surface reaction activities and production profiles are reported. The results presented in Figure 6 display the impact of the catalyst porosity, where it was deduced that the change in the catalyst porosity from 0.99 to 0.50 has significantly influenced the surface reaction activity and the production profiles. Moreover, it was unveiled that both the adsorbed propane (i.e., C_3H_8X) and the adsorbed hydrogen (i.e., HX) was largely stable for an extended period on the surface profiles. In addition, the production profile indicated that the propane consumption rate became more rapid for the 0.50 porosity compared to 0.99 porosity, with 0.50 porosity displaying higher propylene yield compared to 0.99 porosity which is evident in Figure 6. A better rate reported for the 0.50 porosity was found to have fallen within the acceptable validation value in the literature [53] where values less than 0.7 were said to be acceptable.

Statistical evaluation of the parameter effects on the kinetics

The results obtained for the statistical evaluation of the effect and contribution of the parameters (i.e., temperature, pressure, porosity, and flow rate) are presented in Table 2.

Table 2. Effect and contribution of selected parameters on the reaction kinetics

Parameter	Effect, unitless	Contribution, %
Temperature	0.06256	22.6269
Pressure	-0.02567	9.2835
Porosity	-0.17252	62.3959
Flowrate	-0.01574	5.6937
		100.0000

The result obtained for the contribution of the selected parameters in influencing the production rate are presented in the trend: Porosity (-62.40%) > Temperature (+22.63%) > Pressure (-9.28%) > Flowrate (-5.69%). All the selected parameters were found to have contributed negatively to the production rate except for the temperature, which positively promoted the reaction or production rate. It was also deduced that catalyst porosity and reaction temperature significantly influenced the reaction kinetics compared to other parameters like the pressure and reactor flow rate.

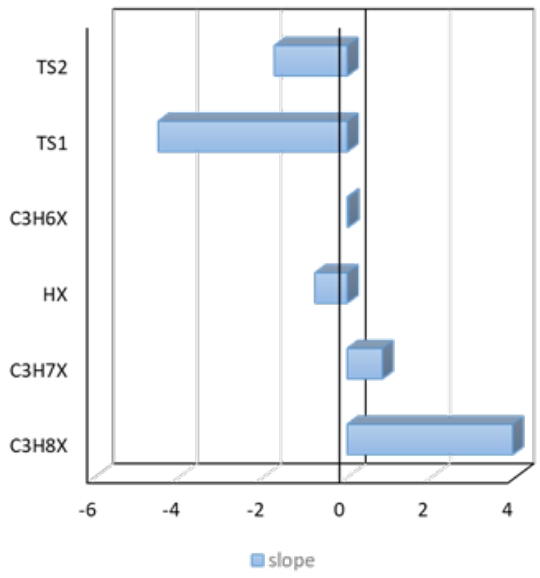

Figure 7. Rate-control analysis profile for the dehydrogenation process steps.

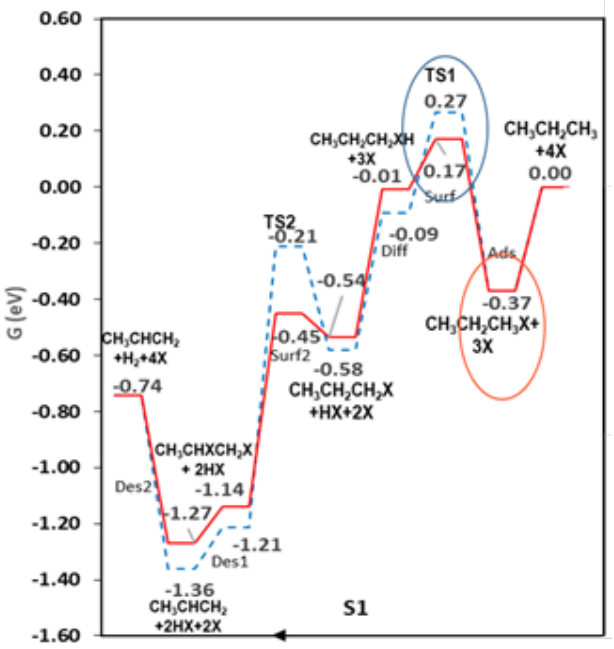

Figure 8. The key reaction state influencing the reaction rate [26].

Rate-control analysis

The results of the reaction rate-control analysis for the propane dehydrogenation reaction network are presented in Figures 7 and 8, showing the impact of each reaction step on the overall kinetics. The findings indicate that the order of rate-control contribution follows the trend: TS1 (first hydrogen abstraction transition state) > C_3H_8X (adsorbed propane) > TS2 (second hydrogen abstraction transition state) > C_3H_7X (adsorbed propyl) > HX (adsorbed hydrogen) > C_3H_6X (adsorbed propylene). Among all the evaluated intermediates and transition states, TS1 exhibited the highest influence, confirming it as the rate-controlling transition state (RC-TS). Similarly, C_3H_8X was identified as the most influential intermediate, designating it as the rate-controlling intermediate state (RC-IS). The identification of TS1 as the RC-TS is consistent with literature reports [17, 54, 55], where the first hydrogen abstraction step was also found to be rate-limiting in studies involving platinum-based catalysts. These key rate-controlling steps—particularly TS1, which had the highest overall impact—should be the primary targets for improving the reaction rate, independent of thermodynamic considerations.

CONCLUSIONS

A micro-kinetic modeling approach was employed in modeling and simulating the kinetics involved in the dehydrogenation process, which was done with a Python-based micro-kinetic code. The results obtained from parametric studies unveil that an increase in reactor flow rate, pressure, and porosity reduces the reaction kinetics. Moreover, the rise in temperature increases the reaction kinetics which confirms the overall reaction to be endothermic, where the impact (i.e., the contribution) of the reactor flow rate, pressure, porosity, and temperature were found to be 5.69, 9.28, 62.40, and 22.63 %, respectively. While the rate control analysis results indicated that among all the intermediate and transition states evaluated, the TS1 (i.e., 1st hydrogen abstraction TS) was identified to have shown the TS with the highest impact, confirming it to be the rate-controlling transition state (RC-TS). At the same time, the C_3H_8X (i.e., adsorbed propane) was found to be the intermediate state with the highest impact, which confirms C_3H_8X, the adsorbed propane, to be the rate-controlling intermediate state (RC-TS). Therefore, among the identified RC-TS and RC-IS, RC-TS was found to have shown the highest impact among all reaction states evaluated, which implies that it would be the most critical reaction state that would significantly have to be used for improving the rate of the reaction outside the potential contributions obtainable from the change in the reaction thermodynamic conditions.

The study, therefore, suggests the improvement of catalyst porosity and possibly impregnation or introduction of catalyst promoters or any other metals [14, 55, 56] to the catalyst surface as a means which would potentially improve the reaction rate

and selectivity outside the potential contributions obtainable from the change in the reaction thermodynamic conditions.

REFERENCES

1. M. Martino, E. Meloni, G. Festa, V. Palma, S. Wacławek, D. Dion, D. Dionysiou, A. Kudelski, J. A. Lauterbach, *Catalysts,* **11***,* 1070 (2021).
2. X. Liang, Z. Mi, Y. Wu, L. Wang, E. Xing, *Reaction Kinetics and Catalysis Letters,* **80** (2), 207 (2003).
3. B. M. Lipinski, L. S. Morris, M. N. Silberstein, G. W. Coates, *J. Am. Chem. Soc.,* **142,** 6800 (2020).
4. Z. Gholami, F. Gholami, Z. Tišler, M. Tomas, M. Vakili, *Energies,* **14***,* 1089 (2021).
5. A. Farshi, F. Shaiyegh, S. H. Burogerdi, A. Dehgan, *Pet. Sci. Technol.,* **29,** 875 (2011).
6. D. Christopher, *Digital Refining Processing, Operations & Maintenance Report,* PTQ Publication, 2013.
7. J. J. Sattler, J. Ruiz-Martinez, E. Santillan-Jimenez, B. M. Weckhuysen, *Chem Rev,* **114,** 10613 (2014).
8. T. Oyegoke, F. N. Dabai, A. Uzairu, B. Y. Jibril, *Hittite Journal of Science & Engineering,* **7**, 297 (2020).
9. A. Benzaouak, H. Mahir, A. Hamidi, M. Kacimi, L. F. Liotta, *Catalysts,* **12,** 811 (2022).
10. S. K. Matam, C. Moffat, P. Hellier, M. Bowker, I. P. Silverwood, C. R. A. Catlow, J. S. David, J. Craswell, P. P. Wells, S. F. Parker, E. K. Gibson, *Catalysts,* **10,** 1370 (2020).
11. A. Zubkov, T. Bugrova, M. Salaev, G. Mamontov, *Crystals,* **11,** 1435 (2021).
12. L. Wang, G. Q. Yang, X. Ren, Z. W. Liu, *Nanomaterials,* **12,** 417 (2022).
13. W. Zhang, H. Wang, J. Jiang, Z. Sui, Y. Zhu, D. Chen, X. Zhou, *ACS Catal.,* **10,** 12932 (2020).
14. R. Zhang, Q. Y. Chang, F. Ma, M. Zeeshan, M. L. Yang, Z. J. Sui, D. Chen, X. G. Zhou, Y. A. Zhu, *Chemical Engineering Journal,* **446,** 136913 (2022).
15. T. Oyegoke, F. N. Dabai, A. Uzairu, B. Y. Jibril, *Bayero Journal of Pure and Applied Sciences,* **11,** 178 (2019).
16. C. F. Li, X. Guo, Q. H. Shang, X. Yan, C. Ren, W. Z. Lang, Y. J. Guo, *Ind. Eng. Chem. Res.,* **59,** 4377 (2020).
17. Q. Li, Z. Sui, X. Zhou, D. Chen, *Appl. Catal. A, Gen.,* **398,** 18 (2011).
18. T. K. Katranas, A. G. Vlessidis, V. A. Tsiatouras, K. S. Triantafyllidis, N. P. Evmiridis, *Microporous and Mesoporous Materials,* **61,** 189 (2003).
19. T. Saelee, S. Namuangruk, N. Kungwan, A. Junkaew, *Journal of Physical Chemistry C,* **122,** 14678 (2018).
20. D. Akporiaye, S. F. Jensen, U. Olsbye, F. Rohr, E. Rytter, M. Rønnekleiv, A. I. Spjelkavik, *Ind. Eng. Chem. Res.,* **40,** 4741 (2021).
21. J. H. Yun, R. F. Lobo, *J. Catal.,* **312,** 263 (2014).
22. J. Schäferhans, S. Gõmez-Quero, D. V. Andreeva, G. Rothenberg, *Chemistry - A European Journal,* **17,** 12254 (2011).
23. M. L. Yang, Y. A. Zhu, X. G. Zhou, Z. J. Sui, D. Chen, *ACS Catal.,* **2,** 1247 (2012).
24. J. Liu , Y. Liu, Y. Ni, H. Liu, W. Zhu, Z. Liu, *Catal. Sci. Technol.,* **10,** 1739 (2020).
25. T. Oyegoke, F. N. Dabai, A. Uzairu, B. Y. Jibril, *Journal of the Serbian Chemical Society,* **86,** 44 (2021).
26. T. Oyegoke, F. N. Dabai, A. Uzairu, B. Y. Jibril, *European Journal of Chemistry,* **11,** 342 (2020).
27. E. E. Peter, T. Oyegoke, A. Y. Atta, A. Uzairu, B. O. Aderemi, B. Muktar, B. Y. Jibril, Computational Design of Metal-Exchanged ZSM-5 Catalyst For Propane Dehydrogenation, *International Conference on Theoretical Aspects of Catalysis,* June 13-17, 2022.
28. S. Chen, Z. J. Zhao, R. Mu, X. Chang, J. Luo, S. C. Purdy, A. J. Kropf, G. Sun, C. Pei, J. T. Miller, X. Zhou, E. Vovk, Y. Yang, J. Gong, *Chem.,* **7,** 387 (2021).
29. C. F. Li, X. Guo, Q. H. Shang, X. Yan, C. Ren, W. Z. Lang, Y. J. Guo, *Ind. Eng. Chem. Res.,* **59,** 4377 (2020).
30. J. Lin, M. Shen, C. Zhang, S. Bi, G. Shen, F. Gao, W. Li, *Chemical Engineering Journal,* **519,** 165243 (2025).
31. T. Oyegoke, F. N. Dabai, S. M. Waziri, A. Uzairu, B. Y. Jibril, *Physical Sciences Reviews,* **9,** 1049 (2024).
32. T. Oyegoke, F. N. Dabai, S. M. Waziri, A. Uzairu, B. Y. Jibril, *Sustainable Chemistry Research,* **1,** 1 (2023).
33. S. Rimaz, L. Chen, S. Kawi, A. Borgna, *Appl. Catal. A, Gen.,* **588,** 117266 (2019).
34. G. Yang, X. Yan, Y. Chen, X. J. Guo, W. Z. Lang, Y. J. Guo, *Appl. Catal. A, Gen.,* **643,** 118778 (2022);
35. M. L. Yang, J. Zhu, Y. A. Zhu, Z. J. Sui, Y. D. Yu, X. G. Zhou, D. Chen, *J. Mol. Catal. A, Chem.,* **395,** 329 (2014).
36. J. Zhang, T. Yu, J. He, J. Chen, G. Wang, Z. Shi, F. Yang, J. Zhao, R. Zhuo, R. Wang, *Molecular Catalysis,* **553,** 113717 (2024).
37. B. B. Li, H. Y. Ma, G. C. Wang, *Langmuir,* **40,** 19043 (2024).
38. H. Y. Ma, G. C. Wang, *Molecular Catalysis,* **563**, 114253 (2024).
39. T. H. Kim, K. H. Kang, M. Baek, J. H. Song, U. G. Hong, D. S. Park, W. C. Choi, Y. K. Park, I. K. Song, *Molecular Catalysis,* **433,** 1 (2017).
40. L.H. Sprowl, C. T. Campbell, L. Árnadóttir, *Journal of Physical Chemistry C*, **120,** 9719 (2016).
41. C. T. Campbell, L. H. Sprowl, L. Árnadóttir, *Journal of Physical Chemistry C,* **120,** 10283 (2016).
42. L. H. Sprowl, C. T. Campbell, L. A. Rnadóttirrnadóttir, *Journal of Physical Chemistry C,* **121,** 9655 (2016).
43. I. A. W. Filot, Introduction to Microkinetic Modeling, Technische Universiteit Eindhoven, 2018.
44. S. Fogler, Essentials of Chemical Reaction Engineering, Prentice Hall, 2010.
45. M. E. Davis, R. J. Davis, Fundamentals of Chemical Reaction Engineering, Dover Publications, 2013.
46. C. T. Campbell, *ACS Catal,* **7,** 2770 (2017).

47. C. Stegelmann, A. Andreasen, C. T. Campbell, *J. Am. Chem. Soc.,* **131,** 13563 (2009).
48. T. Otroshchenko, G. Jiang, V. A. Kondratenko, U. Rodemerck, E. V. Kondratenko, *Chem. Soc. Rev,* **50,** 486 (2021).
49. W. Wannapakdee, T. Yutthalekha, P. Dugkhuntod, K. Rodponthukwaji, A. Thivasasith, S. Nokbin, T. Witoon, S. Pengpanich, C. Wattanakit, *Catalysts,* **9** (2)**,** 174 (2019).
50. N. Raman, S. Maisel, M. Grabau, N. Taccardi, J. Debuschewitz, M. Wolf, H. Wittkämper, T. Bauer, M. Wu, M. Hauman, C. Papp, A. Görling, E. Spiecker, J. Libuda, H. P. Steinrück, P. Wasserscheid, *ACS Catal.,* **9,** 9499 (2019).
51. I. M. Mándity, S. B. Ötvös, F. Fülöp, *ChemistryOpen,* **4,** 212 (2015).
52. G. Laudadio, N. J. W. Straathof, M. D. Lanting, B. Knoops, V. Hessel, T. Noël, *Green Chemistry,* **19,** 4061 (2017).
53. Purdue, Gradient Check for Heterogeneous Catalysis Purdue University*,* 2016.
54. A. W. Hauser, P. R. Horn, M. Head-Gordon, A. T. Bell, *Physical Chemistry Chemical Physics,* **18**, 10906 (2016).
55. T. Oyegoke, F. N. Dabai, S. M. Waziri, A. Uzairu, B. Y. Jibril, *Kemija u industriji,* **71,** 583 (2022).
56. N. F. Kalantari. M. Bekheet, K. N. P. Delir, J. O. Back, A. Farzi, S. Penner, N. Delibaş, S. Schwarz, J. Bernardi, D. Salari, A. Niaei, *Journal of Industrial and Engineering Chemistry,* **111,** 168 (2022).